

The $^{88}\text{Sr}(p,\gamma)^{89}\text{Y}$ reaction at astrophysically relevant energies

S. Galanopoulos, P. Demetriou, M. Kokkoris, and S. Harissopoulos

Institute of Nuclear Physics, National Centre for Scientific Research "Demokritos," P.O. Box 60228, 153.10 Aghia Paraskevi, Athens, Greece

R. Kunz, M. Fey, and J. W. Hammer

Institut für Strahlenphysik, Universität Stuttgart, Allmandring 3, 70569 Stuttgart, Germany

Gy. Gyürky, Zs. Fülöp, and E. Somorjai

Institute of Nuclear Research of the Hungarian Academy of Sciences (ATOMKI), Bem tér 18/c, 4001 Debrecen, Hungary

S. Goriely

Institut d'Astronomie et d'Astrophysique, Université Libre de Bruxelles, Campus de la Plaine, CP226, 1050 Brussels, Belgium

(Received 21 May 2002; published 9 January 2003)

The cross section of the $^{88}\text{Sr}(p,\gamma)^{89}\text{Y}$ reaction was determined by in-beam measurements at energies $E_p = 1.4\text{--}5$ MeV relevant to the nucleosynthetic p process. At $E_p \geq 3.5$ MeV, the γ angular distributions were obtained by using one HPGe detector of 80% relative efficiency, whereas at $E_p \leq 3.5$ MeV they were measured by means of an array of four HPGe detectors all shielded with BGO crystals for Compton background suppression. Three of them had a relative efficiency $\epsilon_r \approx 100\%$, whereas the remaining one had $\epsilon_r \approx 78\%$. From the resulting cross sections, that lie in the $0.5\text{--}\mu\text{b--}5\text{--mb}$ range, astrophysical S factors and reaction rates have been derived. Cross sections, S factors, and reaction rates have also been calculated by means of the statistical model code MOST. A very good agreement between the experimental data and the theoretical predictions has been found.

DOI: 10.1103/PhysRevC.67.0158XX

PACS number(s): 25.40.Lw, 26.30.+k, 27.60.+j, 97.10.Tk

I. INTRODUCTION

Despite the impressive progress that has been made in recent years in improving our understanding of the solar system nuclidic composition, there remain puzzles that challenge the basis of theoretical modeling as well as of experimental approaches. Among these puzzles, the origin of the so-called p nuclei is still a major one. The term p nuclei refers to the 35 stable proton-rich nuclides shown in Fig. 1, that lie on the "northwest" side of the stability valley on the chart of nuclides, between ^{74}Se and ^{196}Hg . In contrast to all the other nuclei that are heavier than iron, p nuclei cannot be synthesized by the two neutron capture processes referred to as s and r processes (see, e.g., Refs. [1–3]). In the development of the theory of nucleosynthesis, it was realized very early that the production of the p nuclei requires a special mechanism, termed the p process [3,4]. This nucleosynthetic scenario involves more or less complicated sequences of neutron, proton, and α -particle photodisintegrations, as well as (p,γ) and (α,γ) reactions. According to p -process models, p nuclei can be synthesized from the "burning" of pre-existing more neutron-rich nuclei at stellar environments of high enough temperature ($T \geq 2 \times 10^9$ K). Such temperature conditions are believed to be fulfilled in the O/Ne layers of massive stars during their pre-supernova phase [5,6] or during their explosion as type-II supernovae [6–8].

Although various p -process calculations have been successful [6,8–14] in reproducing the abundances of a variety of p nuclei, this is not the case in, e.g., the $A \approx 90$ mass region, where the predictions severely underproduce the Mo and Ru p nuclei. Serious problems are also encountered in

other mass regions. These discrepancies could be attributed to uncertainties in the modeling of the preceding slow neutron-capture process [14] or in the description of the stellar evolution [15]. In addition to the uncertainties of the astrophysical modeling, nuclear physics uncertainties can also affect the calculations of the solar system abundances of the p nuclei. This is due to the fact that the understanding of these abundances requires extended network calculations (see, e.g., Ref. [9]) involving more than 20 000 nuclear reactions with about 2000 nuclei in the mass region $12 \leq A$

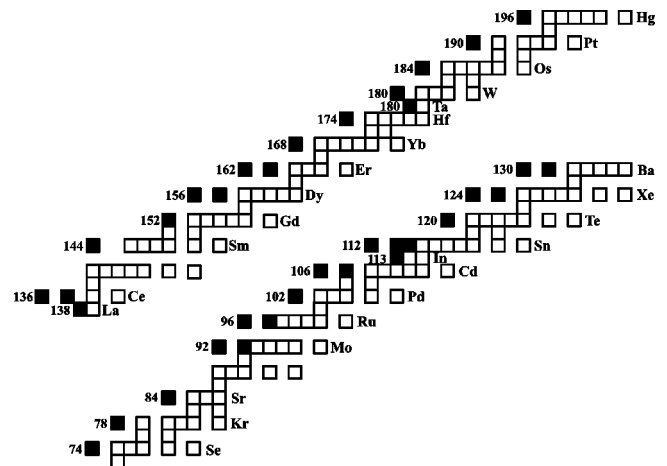


FIG. 1. Chart of the stable nuclides (boxes) from As ($Z=33$) to Hg ($Z=80$). The p nuclei are indicated with black boxes. Symbols are displayed only for the elements with p isotopes. The number shown for each element is the mass number A of the corresponding lightest isotope.

≤ 210 . In this reaction network, the reactions $^{12}\text{C}(\alpha, \gamma)^{16}\text{O}$ and $^{22}\text{Ne}(\alpha, n)^{25}\text{Mg}$ have proved to have an important contribution [16] since they strongly affect [17,18] the production of the “seed” s -process nuclei from which p nuclei can be synthesized via various neutron, proton, and α -particle photodisintegrations. Furthermore, the role of the Hauser-Feshbach (HF) theory [19] in p -process calculations is also crucial: abundance calculations have to rely almost completely on the predictions of the HF theory since it is hardly possible to measure the cross sections of all the reactions involved in the huge network mentioned above. A very important step in the investigation of nuclear physics uncertainties involved in any p -nuclei abundance calculations is to perform a validity test of the statistical HF model in the mass region of interest. One should of course emphasize that the uncertainties involved in the HF calculations are not related to the HF theory itself, but rather to the uncertainties in the evaluation of the nuclear properties entering the calculations. These properties are the nuclear masses, the nuclear level densities (NLDs), the nucleon-nucleus and α -nucleus optical model potentials (OMPs), and finally the γ -ray strength functions.

A sensitive check of the reliability of the HF calculations can be performed by comparisons with experimental cross sections. The main problem hereby is the lack of experimental data. Compared to the huge number of reactions required for p -process studies, the amount of existing data is proportionally very small. In fact, very few experimental works have been reported on cross section measurements in the mass region from Se to Sn [20–28]. Given these facts, additional laboratory work, like the present one, aiming at determining cross sections at energies relevant to p process is strongly required.

In addition to the data needs mentioned above, the present work has also been motivated by the recent investigations of Gyürky *et al.* [28] in which the proton-capture cross sections of the ^{84}Sr , ^{86}Sr , and ^{87}Sr isotopes were simultaneously measured by means of the activation technique. The resulting S factors of ^{84}Sr were found to be in very good agreement with the HF predictions, whereas deviations were observed in the case of ^{86}Sr and ^{87}Sr . In view of these findings, the determination of the proton-capture cross section of the heavier $N = 50$ ^{88}Sr isotope is of paramount importance, as it will help to clarify whether the discrepancies between theory and experiment observed in Ref. [28] have a tendency to increase as the nuclei approach the $N = 50$ shell closure.

II. EXPERIMENTAL PROCEDURES

The present measurements have been carried out at the 4-MV single-ended DYNAMITRON accelerator of the University of Stuttgart as well as at the 5.5-MV T11 Van de Graaff Tandem accelerator of the National Research Center “Demokritos,” Athens. In Stuttgart, measurements were carried out at beam energies from 1.4 to 3.5 MeV, whereas in Athens the energy region from 2.6 to 5 MeV was additionally covered. Both accelerators have been calibrated in the beginning of the respective measurements with the 992-keV resonance of the $^{27}\text{Al}(p, \gamma)^{28}\text{Si}$ reaction.

Gamma-singles spectra were taken using the same target in all runs. This was produced by evaporating $^{88}\text{Sr}(\text{NO}_3)_2$ powder on a 0.4-mm-thick tantalum backing. The target material was 99.84% enriched in ^{88}Sr . The amount of ^{88}Sr in the target was determined by means of an XRF analysis before all measurements. It was also checked at the end of the Stuttgart measurements as well as at the end of the Athens runs. The thickness of ^{88}Sr in the target before any measurement was $168 \pm 7 \mu\text{g}/\text{cm}^2$, and the material loss was found to be less than 3%. This thickness corresponds to approximately 12 and 8 keV at beam energies of 2 and 4 MeV, respectively. These values were derived using the SRIM code [29], and assuming that the target consists of ^{88}Sr only. However, the thickness of the target is defined by its stoichiometry that was determined at the end of the measurements by performing a nuclear reaction analysis (NRA). In our case, it is expected that during the evaporation a significant loss of N occurs due to the escape of NO and NO_2 gases. Therefore, after the exposure of the target in atmospheric conditions and humidity, the resulting stoichiometry is different from that before the evaporation procedure. The resulting chemical composition usually comprises of different phases. Due to these effects, the NRA measurements were necessary to determine correctly the proton stopping powers, i.e., the beam energy losses in the target and, hence, to reduce the uncertainties in the calculations of effective beam energies before transforming them into center-of-mass energies. The NRA measurements were performed using a single-charged ^2H beam of 1.1-MeV energy that was delivered by the Tandem accelerator of “Demokritos,” Athens. Hereby, the $^{14}\text{N}(d, \alpha_1)^{12}\text{C}$ reaction was used to determine the amount as well as the distribution of nitrogen in the target. The beam spot was $2 \times 2 \text{ mm}^2$ wide, and the beam current on the target did not exceed 10 nA due to pile-up considerations. A total charge of $64 \mu\text{C}$ was accumulated. A silicon surface barrier detector, having a resolution of 14 keV, was placed at 150° with respect to the beam in order to obtain a better depth resolution.

The NRA cross-section data necessary for the analysis of the spectra resulting from the $^{14}\text{N}(d, \alpha_1)^{12}\text{C}$ reaction were taken from Ref. [30]. This reaction produces an isolated peak in the high energy part of the spectrum, and can be separated from all other nuclear reactions coming either from the ^{16}O present in the target or from any low- Z contaminant, such as ^{12}C . Spectra were taken for three different target areas along the radius of the target disk. A typical spectrum taken by impinging the ^2H beam on the center of the target is shown in Fig. 2, which is divided in three parts. Part *a* corresponds to the yield of the elastically scattered deuterons by the target. The peak shown in part *b* results from the $^{12}\text{C}(d, p)^{13}\text{O}$, $^{16}\text{O}(d, p_{0,1})^{17}\text{O}$, and $^{14}\text{N}(d, p)^{15}\text{N}$ reactions that could not be resolved in our case. In part *c* two peaks are shown. They both arise from the $^{14}\text{N}(d, \alpha_1)^{12}\text{C}$ reaction. The analysis of the spectra has shown that the peak labeled with 1 is due to the adsorption of the NO and NO_2 gases on the Ta backing. This obviously occurred in the beginning of the evaporation of the $^{88}\text{Sr}(\text{NO}_3)_2$ powder. The peak labeled with 2 was found to arise from the amount of ^{14}N “left” in the target. Hence the analysis of the spectra yielded the nitrogen deple-

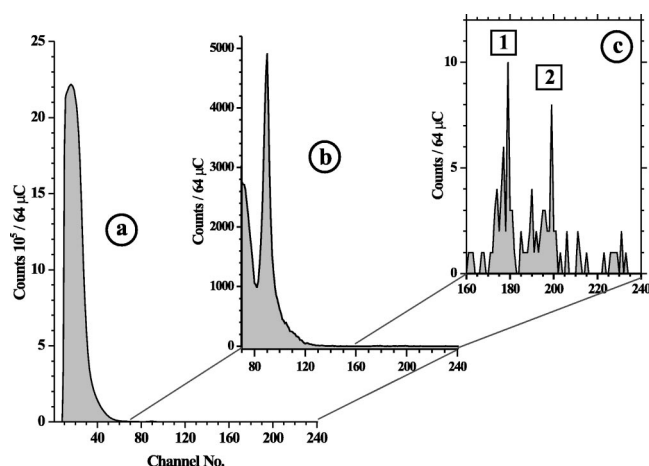


FIG. 2. Typical RBS/NRA spectrum taken by using a 1.1-MeV ^2H beam impinging on the target used (see the text for details).

tion as well as the atomic ratio N/Sr in the target. This ratio was found to be less than 3.5% at the center of the target and $\approx 2\%$ at a distance of about 1 cm from it. Obviously the target was slightly inhomogeneous along its radius. Moreover, from the analysis of the spectra we could conclude that the target comprised of two phases, namely, the $^{88}\text{Sr}(\text{NO}_3)_2$ the $^{88}\text{Sr}(\text{OH})_2$ phases. Furthermore, the amount of the former phase was found to be very small ($\leq 4\%$). It has to be noted that the formation of the SrO phase is not favorable due to the strong alkaline behavior of Sr. In our case, this has been verified not only by the analysis of the NRA spectra but also from the optical controls of the target after the evaporation as suggested in Ref. [31]. Obviously, the stoichiometry of the target might change not only during the evaporation, but also during the ion bombardment. Hence the results of the NRA could differ from those obtained herein if the target were analyzed in the beginning of the measurements. The fact however that the final amount of ^{88}Sr in the target, according to the XRF analyses, did not differ practically from that in the beginning of the measurements allows us to calculate the maximum total target thickness by varying the ratio of the amount of the $^{88}\text{Sr}(\text{NO}_3)_2$ to the $^{88}\text{Sr}(\text{OH})_2$ phase. The maximum thickness obtained this way is $405 \mu\text{g}/\text{cm}^2$, that corresponds to 44 and 28 keV at 2 and 4 MeV, respectively. This thickness is derived if the target is comprised of the $^{88}\text{Sr}(\text{NO}_3)_2$ phase only. Even in such an extreme case the uncertainty entering the determination of the corresponding effective energies is less than 0.5%.

The experimental setup used in Stuttgart for the cross section measurements at $E_p \leq 3.5$ MeV (described briefly in Ref. [32]) is shown in Fig. 3. It consisted of four large volume HPGe detectors, all shielded with BGO crystals for Compton background suppression. Three of them had a relative efficiency $\epsilon_r \approx 100\%$, whereas the remaining one had $\epsilon_r \approx 78\%$. The current of the proton beam was about $10 \mu\text{A}$. The target was placed at 90° to the beam axis. Its backing was cooled directly with water during the whole experiment. The beam spot had a diameter of ≈ 4 mm. The detectors were placed on a rotating table at distances between 10 and 20 cm from the target. By rotating the table by 15° γ -single spectra

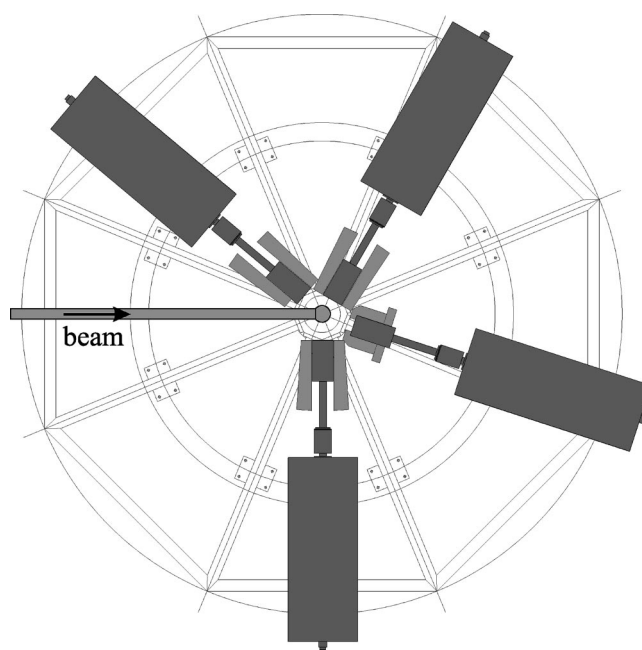


FIG. 3. Graph of the setup used in the present work for the cross section measurements at $E_p \leq 3.5$ MeV (Stuttgart). An array of four BGO-shielded Ge detectors (shaded areas) was placed on a motor-driven table that was rotating by 15° in order to measure γ -single spectra at eight angles.

were measured at eight angles with respect to the beam direction. In this way, the angular distributions of the γ rays of interest were determined in the energy range $E_p = 1.4$ – 3.5 MeV, with a step of 100 keV. This task was repeated at each energy point with the proton beam impinging on a blank Ta backing, in order to investigate possible yield contributions from reactions occurring in the backing material. The absolute efficiency of the setup was determined at all eight angles by taking spectra from calibrated radioactive sources (^{60}Co , ^{133}Ba , ^{152}Eu , ^{226}Ra) and from the $^{27}\text{Al}(p, \gamma)^{28}\text{Si}$ reaction at the plateau of the 992-keV resonance. From the latter reaction, relative efficiency curves were first determined using the branchings reported by Anttila *et al.* [33] for γ rays up to $E \approx 12$ MeV. These branchings agree within 5% with those reported by Endt *et al.* [34]. The relative efficiency curves obtained from the $^{27}\text{Al}(p, \gamma)^{28}\text{Si}$ reaction were then matched to the absolute efficiencies obtained with the sources.

In the cross section measurements carried out in Athens, spectra were taken using one HPGe detector without any BGO shields. The target was placed at 20° with respect to the beam axis. The beam current was $\approx 1.3 \mu\text{A}$ and the beam spot was $\approx 2 \times 2 \text{ mm}^2$. The distance between the target-center and the detector-front was 12 cm. The detector was placed on a goniometric table that could rotate around the target with an accuracy better than 1° . In order to measure γ angular distributions at each beam energy, γ -singles spectra were taken at six angles with respect to the beam. The target backing was cooled with air during all measurements. As in the case of the measurements in Stuttgart, background spectra were also measured, in order to investigate possible yield contributions from the backing material. Moreover, the abso-

lute efficiency of the setup used was determined at each one of the six angles by the same procedure that was applied in the Stuttgart runs. In both the Stuttgart and Athens experiments, the absolute efficiency data were checked for uncertainties due to coincident summing according to the procedure described in Ref. [35]. For this check, an additional ^{57}Co radioactive source was used. In both cases, this effect was found to be negligible ($\leq 1\%$). Moreover, a detailed analysis of the γ spectra measured has shown that these are not affected by coincident summing. This result was actually expected since the detectors used were placed at a proper long distance from the target.

III. DATA ANALYSIS AND RESULTS

In order to determine the cross section of the $^{88}\text{Sr}(p, \gamma)^{89}\text{Y}$ reaction, the absolute yield of all the γ transitions feeding the ground state of the produced ^{89}Y has to be derived, i.e. the angular distributions of all these γ transitions have to be measured. As shown in Fig. 4(a), the excited states of the produced ^{89}Y nucleus can be populated by γ transitions deexciting higher lying discrete levels (*secondary γ rays or cascade feeding*) as well as the entry state (*primary γ rays or direct feeding*).

When considering the ground state, the direct feeding results in the so-called γ_0 transition, i.e., a γ ray from the “entry” level having an excitation energy of $E_X = Q + E_{c.m.}$ to the ground state is present in the spectra. At this point, it has to be emphasized that one actually populates more than one “entry” state. At such high excitation energies ($E_X \geq Q = 7.07$ MeV) the level density of the produced compound nucleus is very high, i.e., the average spacings between the excited levels are less than some hundreds of eV. Hence the produced compound nuclei can be found in many excited states lying in an energy window δE , whose width depends on the thickness of the target used (being usually some tens of keV at least) and the beam energy spread that is much smaller (typically in the order of 1–3 keV). Hence, the γ_0 transition is the result of the decay of all the “entry” states populated by the reaction to the ground state. In the following, the direct feeding to the first excited level L_1 [see Fig. 4(a)] will be referred to as the γ_1 transition, the one to the second excited state L_2 as the γ_2 transition, and so on. Here the γ rays observed in the spectra were properly assigned to γ transitions of ^{89}Y according to the compilation of Firestone *et al.* [36]. This task was carried out not only for the γ transitions observed in ^{89}Y , but also for those that might be present as the result of contaminant reactions that can occur due to the composition of the target as well as of the backing material. From the analysis of the spectra it was found that the γ_0 transition together with 11 other secondaries are those γ rays that contribute significantly ($\geq 97\%$) to the absolute yield of the reaction. These γ transitions are shown in Fig. 4(b). In the present work, the absolute yield of all these γ transitions was measured at all angles and all beam energies. From these yields, the relevant γ angular distributions $W(\theta)$ were determined.

A typical γ -single spectrum taken at $E_p = 3$ MeV is shown in Fig. 5, whereas in Fig. 6 all $W(\theta)$'s that were determined

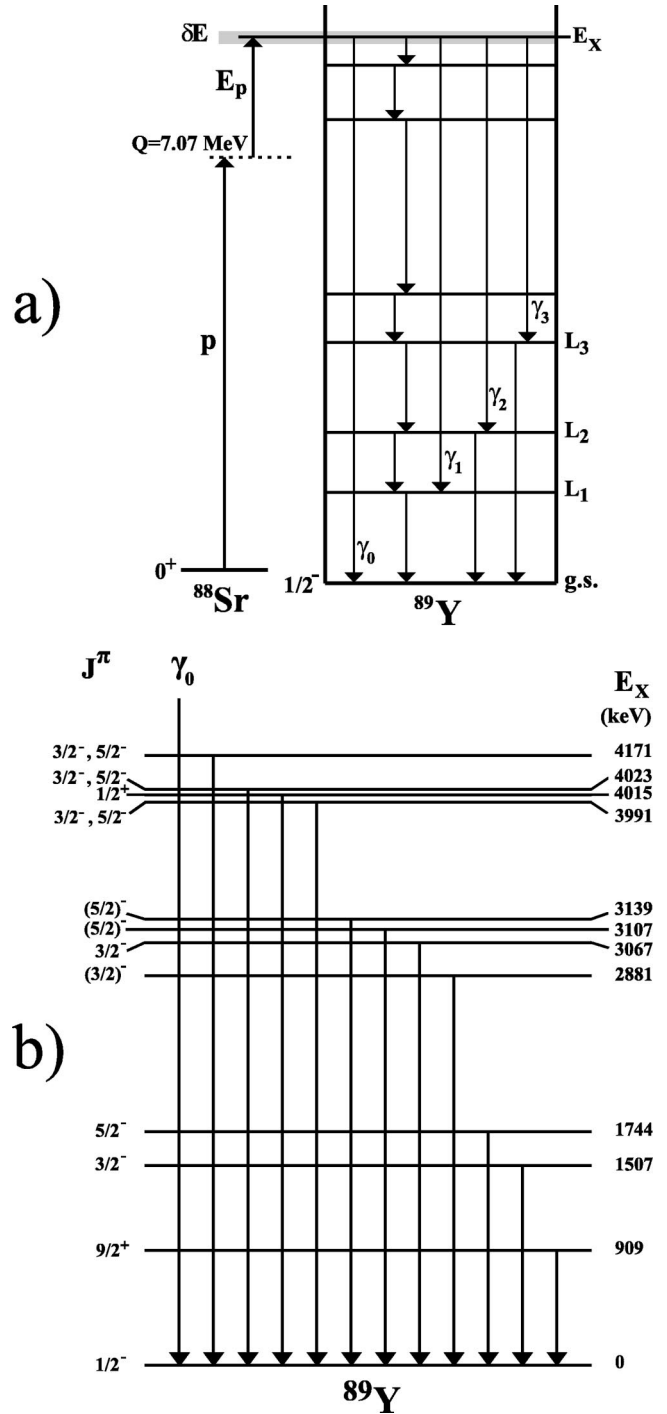


FIG. 4. (a) Simplified level diagram of the ^{89}Y nucleus (see the text). (b) Partial level scheme of the ^{89}Y nucleus showing all the γ transitions which were observed to populate its ground state. They were all taken into account in the determination of the cross section. The excitation energies E_X , as well as the spins and parities shown were adopted from the compilation of Firestone *et al.* [36].

at $E_p = 2.5$ MeV are shown as typical examples of the present work. It has to be emphasized that due to the high efficiency of the setup used, we were able to observe most of the direct feeding transitions up to, at least, the 20th excited discrete level—according to the level listing of Firestone

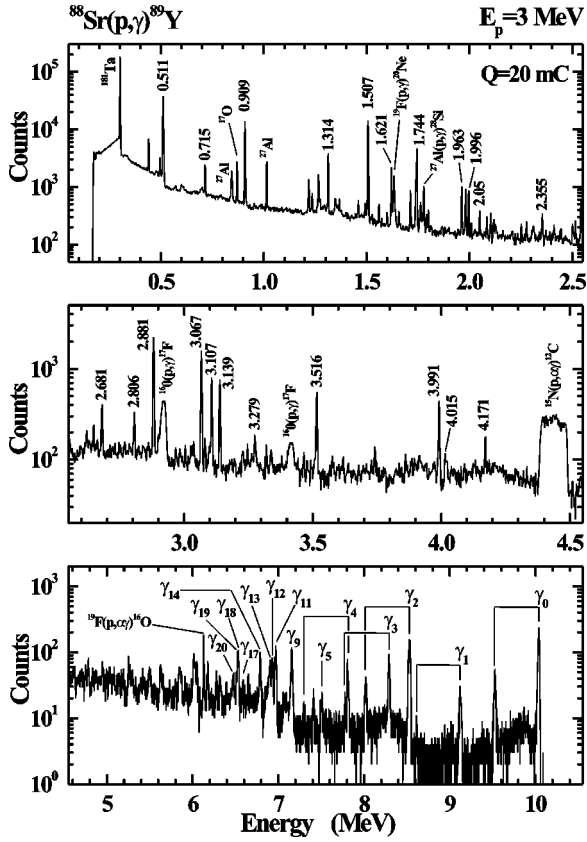


FIG. 5. Typical γ spectrum measured at $E_p = 3$ MeV with the Ge detector placed at 90° . The accumulated charge was 20 mC. The strong secondary γ transitions de-populating excited states of the ^{89}Y nucleus are labeled with numbers corresponding to their energies in MeV (upper and middle parts). The strongest primary γ transitions are shown in the lower part. The first escape peaks of the γ_0 , γ_1 , γ_2 , γ_3 , and γ_4 transitions are also indicated.

et al. [36]—of the produced ^{89}Y nucleus. These primary γ rays are shown in the lower part of Fig. 5. They are labeled as γ_0 , γ_1 , γ_2 , γ_3 , and so on. It has to be noted that the total cross section could also be obtained from the intensities of the primary transitions alone. In this analysis, we chose not to apply this method so as not only to avoid errors due to the proton decay of unbound states after compound nucleus formation but also to avoid systematic errors arising from uncertainties in the level schemes often encountered at high excitation energies. In the latter cases, the primaries deexciting the entry state can be many more than the ones seen by the detector. This can potentially be a very serious problem since many of these primary γ rays are very weak and can have, in addition, high energy, which makes their detection by a Ge detector with poor efficiency rather difficult. For these reasons we used, apart from the γ_0 transition, the angular distributions of the secondary γ transitions feeding the ground state. The analysis of the angular distributions gave for each γ transition the corresponding “absolute” A_0 coefficient. The influence of solid angle effects were investigated according to the procedure described in Ref. [37] and the resulting uncertainties in the A_0 coefficients were found to be of the order of 4%. In the analysis of the angular distribu-

tions of some high energy γ lines with poor statistics, these effects yielded uncertainties up to 8%. The total cross section was deduced from

$$\sigma_T = \frac{A}{N_A} \frac{1}{\xi} \sum_{j=1}^{12} A_0^j, \quad (1)$$

where A is the atomic weight of ^{88}Sr , N_A is Avogadro's number, and ξ is the thickness of ^{88}Sr in the target. The resulting cross sections σ_T given in units of μb are summarized in Table I. The total errors given in Table I for σ_T range from 8% to 20%. Apart from the errors due to statistics, we took into account errors of 5%, 4%, and 3% due to charge, target thickness and efficiency measurements, respectively. The solid angle corrections introduced an average error of $\approx 4\%$. All these errors were added quadratically with the statistical errors. The latter ones are $\approx 1\%$ at beam energies $E_p \geq 2.5$ MeV and $\approx 2\%$ for E_p ranging from ≈ 2 to 2.5 MeV. At energies below 2 MeV, the statistical errors can vary from 2% to 5%. Hence the relative contribution of the different sources of uncertainties to the final total error given in Table I is on average as follows: charge measurement $\approx 30\%$, solid angle effects and target thickness XRF measurements $\approx 25\%$ each, absolute efficiency measurements $\approx 18\%$, and count rate statistics $\approx 2\%$.

The energies given in the first column of Table I are the effective energies in the center-of-mass system. They were determined by using appropriate stopping powers [29], and were subsequently transformed to the center-of-mass system. The corresponding astrophysical S factors have been calculated by using

$$S(E) = \sigma_T(E) E e^{2\pi\eta}, \quad (2)$$

where η is the Sommerfeld parameter and $\sigma_T(E)$ is the total cross section at the center-of-mass energy E . The results are included in Table I.

IV. DISCUSSION

Nuclear reactions occurring at energies up to several MeV are known to proceed through the formation and decay of a compound nucleus system. After reaching equilibrium the compound system eventually decays to various states independent of the entrance channel. The probability of decay into one of the decay channels is described by the HF theory [19], and is given by

$$\sigma_{\alpha\beta} = \pi \chi_\alpha^2 \frac{1}{(2I+1)(2i+1)} \sum_{J^\pi} (2J+1) \frac{T_\alpha^{J^\pi} T_\beta^{J^\pi}}{\sum_{\alpha'} T_{\alpha'}^{J^\pi}}, \quad (3)$$

where α and β denote the entrance and decay channels, respectively, I and i are the target and projectile spins, respectively, and $T_{\alpha\beta}^{J^\pi}$ are the transmission coefficients summed over all orbital and channel spins to give the total transmission coefficient for the formation of the compound nucleus in the state J^π . When the compound nucleus is excited to states

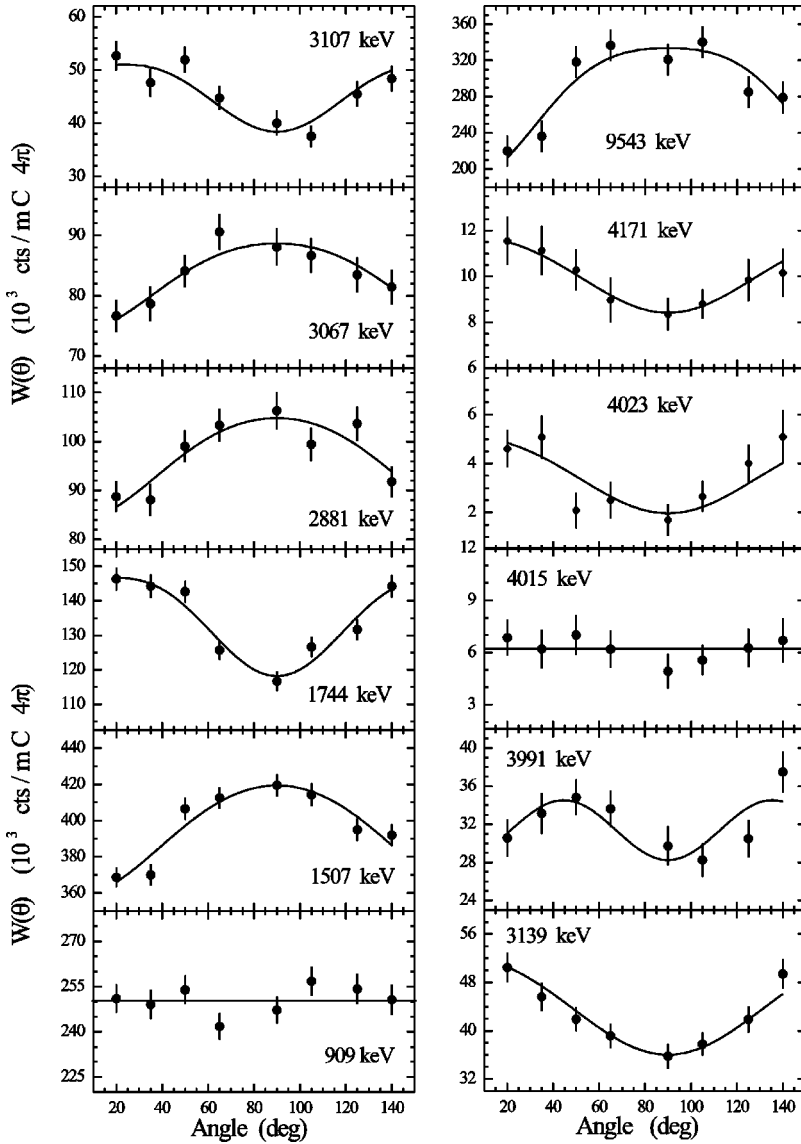


FIG. 6. Angular distributions of all 12 γ transitions observed to contribute to the cross section at $E_p = 2.5$ MeV. The solid curves correspond to the Legendre polynomials fitted to the data points in order to deduce the absolute A_0 coefficients. Based on the multiplicities given in Ref. [36], the data points of the 1507- and 3067-keV γ rays were fitted with Legendre polynomials of first degree, whereas for the remaining γ transitions Legendre polynomials of second degree were used. As shown, the 909- and 4015-keV γ transitions are isotropic. The former one de-excites an isomeric state with $T_{1/2} = 16.06$ s, whereas the latter one depopulates an excited level with spin $J = \frac{1}{2}$. The γ_0 transition observed at $E_p = 2.5$ MeV has an energy of 9543 keV. Its angular distribution is plotted in the upper-right part of the figure.

in the continuum the transmission coefficients in Eq. (3) are replaced by averaged transmission coefficients obtained from an integral over a specified level density. The theoretical S factors are then obtained by inserting the cross sections of Eq. (3) into Eq. (2) of the Sec. III.

Compound nucleus emission depends primarily on the transmission coefficients and the nuclear level densities of the residual nuclei. The transmission coefficients for particle emission are calculated from the appropriate optical model potentials. The photon transmission function is calculated assuming the dominance of dipole transitions and the electric- and magnetic-dipole transition strength functions are usually described by a Lorentz-type function where the energies and widths are determined by experimental data or by appropriate parametrizations. The nuclear level densities can be derived from phenomenological models or from microscopic calculations taking into account the discrete structure of the single-particle spectra associated with realistic effective potentials. The latter treat shell, pairing, and deformation effects consistently, whereas in the former they are considered by means of empirical corrections.

A. S factors

In this section we compare the S factors of the $^{88}\text{Sr}(p, \gamma)^{89}\text{Y}$ reaction obtained in the present measurements with the ones derived from the HF cross sections calculated by the statistical model code MOST [38]. This code includes all available experimental information on nuclear masses, deformation, and spectra of low-lying states. Different parametrizations can be used in principle, for the giant dipole strength functions, the nucleon and alpha-particle OMPs, as well as for NLDs leading to different cross section predictions. In our approach, we use nuclear masses from the experimental compilation of Audi and Wapstra [39] and the ground-state properties (matter density, single-particle level scheme) predicted from the microscopic Hartree-Fock-BCS (HFBCS) model [40]. The NLDs are derived from microscopic statistical calculations [41,42] based on the resulting Hartree-Fock-BCS level scheme [40]. The global alpha-nucleus OMP of Grama and Goriely [43] and the γ -ray strength functions given by Lorentz-type functions according to Refs. [44,45], respectively, are implemented. In the $M1$

TABLE I. Total cross sections σ_T and astrophysical S factors S measured in the present work.

$E_{\text{c.m.}}$ (MeV)	σ_T (μb)	S (10^5 MeV b)
1.379	0.66 ± 0.13	528 ± 104
1.479	0.91 ± 0.14	262 ± 40
1.580	2.2 ± 0.3	251 ± 34
1.680	3.2 ± 0.4	159 ± 20
1.780	8.3 ± 0.9	192 ± 21
1.880	15.6 ± 1.7	180 ± 21
1.982	16.7 ± 1.8	100 ± 11
2.080	48 ± 5	161 ± 17
2.180	60 ± 6	116 ± 12
2.280	136 ± 13	157 ± 15
2.380	158 ± 15	113 ± 11
2.480	168 ± 16	76 ± 7
2.561	206 ± 19	66 ± 6
2.581	198 ± 18	59 ± 5
2.680	365 ± 33	73 ± 7
2.780	413 ± 38	57 ± 5
2.880	527 ± 51	51 ± 5
2.957	613 ± 56	45 ± 4
2.980	667 ± 61	46 ± 4
3.081	1020 ± 91	51 ± 5
3.180	1030 ± 93	38 ± 3
3.281	1280 ± 117	35 ± 3
3.354	1320 ± 124	30 ± 3
3.380	1440 ± 132	31 ± 3
3.478	2080 ± 187	34 ± 3
3.552	1770 ± 168	24 ± 2
3.750	2180 ± 198	18 ± 2
3.948	2930 ± 231	16 ± 1
4.146	3630 ± 298	13 ± 1
4.344	4660 ± 382	12 ± 1
4.541	4210 ± 333	7.3 ± 0.6
4.739	4310 ± 336	5.4 ± 0.5
4.937	2690 ± 222	2.5 ± 0.2

case, the energies and widths are obtained from the latest recommendations of [46]. Four different nucleon-nucleus OMPs, namely, those of Jeukenne *et al.* [47], Bauge *et al.* [48], Koning and Delaroche [49], and Becchetti and Greenless [50] are used. The first two are based on microscopic infinite nuclear matter calculations applied with the local density approximation, while the last two are purely phenomenological.

The results are compared with the experimental data in Fig. 7. The S factors obtained with the OMPs of Refs. [47] (solid line) and [48] (dashed line) are in good agreement with the experimental data, while those of Refs. [49] (dot-dashed line) and [50] (short-dashed line) lead to deviations from the data. The OMP of Ref. [47] combined with the NLD of Ref. [42] seems to give the best description of the data over the whole energy range, whereas small discrepancies are observed at lower energies when the OMP of Ref. [48] is used. Nevertheless, both OMPs (Refs. [47,48]) give S

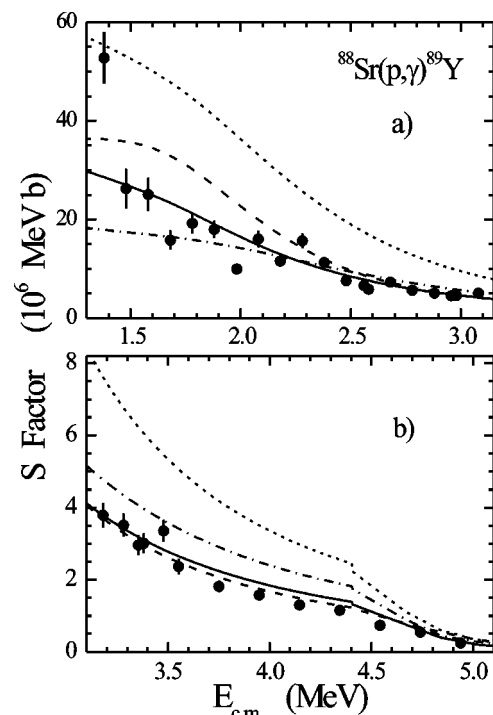


FIG. 7. S factors of the $^{88}\text{Sr}(p, \gamma)^{89}\text{Y}$ reaction measured in the present work (solid circles) compared with the predictions of the statistical model code MOST using different nucleon-nucleus optical model potentials (see the text). The solid line is obtained with the NLD of Ref. [42] and the nucleon OMP of Ref. [47]. The energy region corresponding to the stellar temperatures T relevant to the p process ranges from 1.39 to 4.13 MeV.

factors within the range of two standard deviations of the experimental data, thus they can be considered as suitable for calculations of S factors at low energies. On the other hand, the OMP of Ref. [49] leads to an overproduction of the data at higher energies that extends beyond two standard deviations, while the OMP of Ref. [50] fails completely at all energies. This is not surprising given that the OMP of Ref. [50] was determined from analyses of phase-shifts at much higher energies [also shown in the case of $^{93}\text{Nb}(p, \gamma)^{94}\text{Mo}$ [27]].

As a result of this comparison, the OMPs of Refs. [49,50] shall not be considered in the analysis hereforth, while the other two shall be treated as indistinguishable within the range of uncertainty depicted by the area formed by the corresponding curves—solid and dashed—in Fig. 7. The resulting range of uncertainty is shown in Fig. 8 by the shaded region.

At the energies measured in this work the γ emission channel is by far the dominant one, with the proton and neutron emission ones becoming important only at energies above 4.4 MeV. Consequently, the HF cross section described by formula (3) will depend mainly on the transmission coefficients of the incident proton at $E \leq 4.4$ MeV, whereas at $E \geq 4.4$ MeV the neutron OMP and the NLDs of the residual nuclei will also play a crucial role.

In order to obtain an estimate of the sensitivity of the HF calculations to the NLD formula, especially in the above-mentioned energy range, the $^{88}\text{Sr}(p, \gamma)$ S factors have been

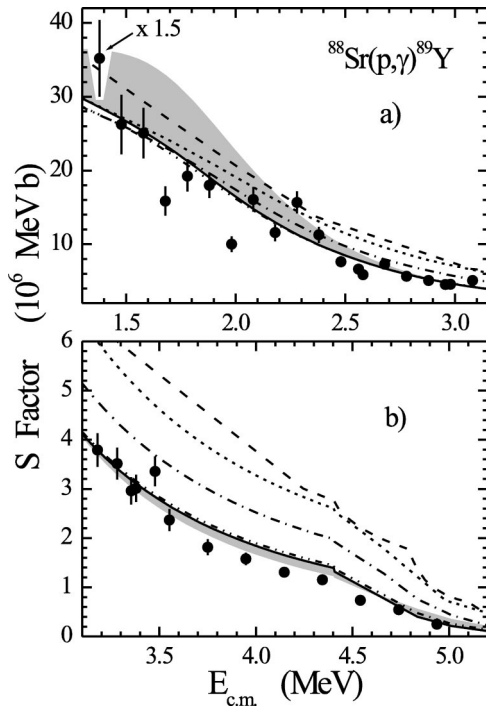


FIG. 8. S factors of the $^{88}\text{Sr}(p,\gamma)^{89}\text{Y}$ reaction measured in the present work (solid circles) compared with the predictions of the statistical model code MOST using different nuclear level densities (see the text). As in Fig. 7, the solid line is obtained with the NLD of Ref. [42] and the nucleon OMP of Ref. [47]. The shaded area reflects the range of uncertainties in the HF calculations due to the optical potentials. Also included are the predictions of Rauscher and Thielemann [54] (dashed line).

calculated using the OMP of Ref. [47] and different NLDs: the back-shifted Fermi gas model NLDs of Goriely [51] and of Thielemann *et al.* [52], and the semimicroscopic ones of Goriely [53] obtained with the extended Thomas-Fermi Strutinsky integral (ETFSI) ground-state properties. The results are compared with the experimental data in Fig. 8. The NLDs of Refs. [42] (solid line) and [53] (dot-dot-dashed line) lead to similar S factors that describe the data well, while those of Refs. [51] (short-dashed line) and [52] (dot-dashed line) overpredict the data at energies above ≈ 2.3 MeV. In fact, the discrepancies observed with the latter NLDs at these higher levels extend well beyond the range of two standard deviations of the experimental data. In other words, overall the uncertainties arising from the NLDs turn out to be larger than those from the OMPs.

In Fig. 8 the S factors are also compared with the global predictions (dashed line) of Rauscher and Thielemann [54], based on the NON-SMOKER code calculations using the OMP of Jeukenne *et al.* [47], the ground-state properties from the finite range droplet model [55] when not available experimentally, and the NLDs from the back-shifted Fermi gas model [56]. An overprediction of the data is observed at energies above ≈ 2.3 MeV similar to that obtained with MOST when using the NLDs of Ref. [51]. This is not surprising since both NLDs are based on the back-shifted Fermi gas model.

To conclude, the combination of the NLD of Ref. [42] or [53] with the OMP of Ref. [47] gives the best reproduction of the experimental data over the whole energy range considered; therefore it can be treated as a recommended set of parameters for the $^{88}\text{Sr}(p,\gamma)^{89}\text{Y}$ cross sections, and the resulting S factors as the recommended S factors for use in astrophysical applications, hereforth. The shaded region in Fig. 8 can, accordingly, be assumed as the range of uncertainty of the above recommended values.

From Figs. 7 and 8, it is obvious that the S factors of the $N=50$ nucleus ^{88}Sr are in very good agreement with the theoretical predictions, in contrast with the results of Ref. [28] for ^{86}Sr and ^{87}Sr . Thus the trend observed in Ref. [28], whereby the discrepancies between theory and experiment increased with increasing value of N (approaching shell closure at $N=50$), is not confirmed by the present analysis. In fact, from all the results on proton capture by the strontium isotopes, reported in Ref. [28] and herein, one cannot infer any systematic behavior along the isotopic chain. The analysis performed with the same set of HF input parameters, i.e., NLDs of Ref. [42] and OMPs of Ref. [47], shows agreement for the isotopes ^{84}Sr and ^{88}Sr , and disagreement for ^{86}Sr and ^{87}Sr . At this point, it is only fair to say that, just as in the case of $^{88}\text{Sr}(p,\gamma)$ (see Fig. 8), the HF calculations for $^{86,87}\text{Sr}(p,\gamma)$ are expected to be affected by large uncertainties due to the lack of experimental information on NLDs and OMPs at the energies of interest. Therefore, the discrepancies observed for $^{86,87}\text{Sr}(p,\gamma)$ could be accounted for by uncertainties in the theoretical predictions. Although it is not yet clear whether these uncertainties arise from the incomplete description of shell, pairing, deformation or other effects, additional systematic studies of (p,γ) and (p,n) reactions, combined with studies of NLDs and OMPs could provide useful insight.

B. Reaction rates

P -process nucleosynthesis is assumed to take place in stellar environments where temperatures between 1.8×10^9 and 3.3×10^9 K are maintained for about 1 s. In the case of the $^{88}\text{Sr}(p,\gamma)^{89}\text{Y}$ reaction these temperature limits correspond to beam energies in the Gamow energy window ranging from 1.39 to 4.2 MeV. This region was completely covered by the present measurements. Therefore, the reaction rates for different temperatures were obtained by

$$\langle \sigma v \rangle = \left(\frac{8}{\pi \mu} \right)^{1/2} \frac{N_A}{(kT)^{3/2}} \int_0^\infty \sigma(E) E \exp\left(-\frac{E}{kT}\right) dE, \quad (4)$$

where $\sigma(E)$ are the cross sections determined experimentally, kT is the thermal energy, E is the center-of-mass energy, and N_A is Avogadro's number.

The results for the laboratory reaction rates obtained with the recommended MOST cross sections are compared with the experimental ones in Fig. 9. A very good agreement between theory and experiment is observed just as in Figs. 7 and 8. The uncertainties in the calculations of the laboratory reaction rates, arising from the uncertainties in the corresponding cross sections, are shown by the shaded area.

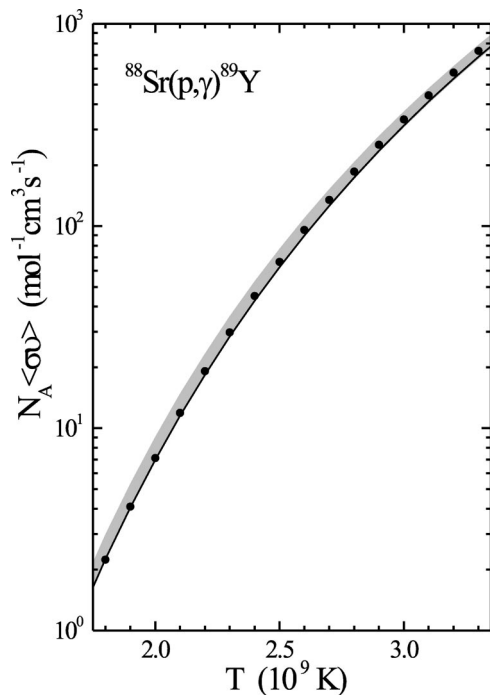


FIG. 9. Rates of the $^{88}\text{Sr}(p, \gamma)^{89}\text{Y}$ reaction vs temperature determined in the present work (solid circles) compared with those predicted by MOST with the NLD of Ref. [42] and the nucleon OMP of Ref. [47] (solid line). The shaded area is the same as in Fig. 8.

V. CONCLUSIONS

In the present work, the total cross sections of the $^{88}\text{Sr}(p, \gamma)^{89}\text{Y}$ reaction were measured at beam energies ranging from 1.4 to 5 MeV, by using in-beam γ -spectroscopy techniques combined with HPGe detectors of very high efficiency, in order to test the predictions of various statistical model calculations in the $N = 50$ mass region. The resulting S

factors were compared with theoretical calculations using different input data.

Of all the sets of NLDs and OMPs used in the HF calculations performed with the code MOST, the NLDs of Demetriou and Goriely [42] and Goriely [53] combined with the nucleon OMP of Jeukenne *et al.* [47] give the best description of the experimental S factors over the whole energy range. The OMP of Bauge *et al.* [48] is almost as successful as the OMP of Ref. [47], apart from some deviations at the lower energies, while those of Koning and Delaroche [49] and Becchetti and Greenlees [50] fail to reproduce the data. Large discrepancies between theory and experiment are observed at energies above 2.3 MeV with the NLDs of Goriely [51] and Thielemann *et al.* [52].

In view of these findings one could conclude that, the S factors, and rates of the $^{88}\text{Sr}(p, \gamma)^{89}\text{Y}$ reaction can be well reproduced within the uncertainty range outlined by the shaded region in Figs. 8 and 9. The recommended input data for the HF calculations are one of the two NLDs: Demetriou and Goriely [42] and Goriely [53] together with one of the following two nucleon OMPs: Jeukenne *et al.* [47] and Bauge *et al.* [48].

Further cross-section measurements of (p, γ) reactions in the Gamow energy window, as well as at energies where many reaction channels compete, will contribute considerably to the systematics required for a globalization of the nuclear input parameters of the HF calculations.

ACKNOWLEDGMENTS

This work was supported by the NATO Collaborative Research Grants Program (Contract No. CRG961086) and the Greek-Hungarian bilateral collaboration program (GSRT/Demokritos/E797 and Tét GR 23/99). We thank Professor Ulrich Kneissl for supporting our work. Zs.F. was supported by Bolyai.

-
- [1] F. Käppeler, F.-K. Thielemann, and M. Wiescher, *Annu. Rev. Nucl. Part. Sci.* **48**, 175 (1998).
- [2] F. Käppeler, *Prog. Part. Nucl. Phys.* **43**, 419 (1999).
- [3] G. Wallerstein *et al.*, *Rev. Mod. Phys.* **69**, 995 (1997).
- [4] N. Prantzos, in *Research Reports in Physics: Nuclear Astrophysics*, edited by M. Lozano, M. I. Gallardo and J. M. Arias (Springer-Verlag, Berlin, 1989), p. 18.
- [5] M. Arnould, *Astron. Astrophys.* **46**, 117 (1976).
- [6] M. Rayet, M. Arnould, M. Hashimoto, N. Prantzos, and K. Nomoto, *Astron. Astrophys.* **298**, 517 (1995).
- [7] M. Arnould, M. Rayet, and M. Hashimoto, in *Unstable Nuclei in Astrophysics*, edited by S. Kubono and T. Kajino (World Scientific, Singapore, 1992), p. 23.
- [8] S. E. Woosley and W. M. Howard, *Astrophys. J., Suppl.* **36**, 285 (1978).
- [9] M. Rayet, N. Prantzos, and M. Arnould, in *Origin and Distribution of the Elements*, edited by G. Mathews (World Scientific, Singapore, 1987), p. 625.
- [10] N. Prantzos, M. Hashimoto, M. Rayet, and M. Arnould, *Astron. Astrophys.* **238**, 455 (1990).
- [11] S. E. Woosley and T. A. Weaver, *Astrophys. J., Suppl.* **101**, 181 (1995).
- [12] A. Heger, R. D. Hoffman, T. Rauscher, and S. E. Woosley, in *Proceedings of the X Workshop on Nuclear Astrophysics*, edited by W. Hillebrandt and E. Müller (MPA, Garching, 2000), p. 105.
- [13] T. Rauscher, A. Heger, R. D. Hoffman, and S. E. Woosley, *Nucl. Phys.* **A688**, 193 (2001).
- [14] V. Costa, M. Rayet, R. A. Zappalà, and M. Arnould, *Astron. Astrophys.* **358**, L67 (2000).
- [15] S. M. Asida and D. Arnett, *Astrophys. J.* **545**, 435 (2000).
- [16] M. Rayet, V. Costa, and M. Arnould, *Nucl. Phys.* **A688**, 74 (2001).
- [17] R. Kunz, M. Fey, M. Jaeger, A. Mayer, J. W. Hammer, G. Staudt, S. Harissopulos, and T. Paradellis, *Astrophys. J.* **A567**, 643 (2002).
- [18] M. Jaeger, R. Kunz, A. Mayer, J. W. Hammer, G. Staudt, K. L. Kratz, and B. Pfeiffer, *Phys. Rev. Lett.* **87**, 202501 (2001).

- [19] W. Hauser and H. Feshbach, *Phys. Rev.* **87**, 366 (1952).
- [20] C. E. Laird, D. Flynn, R. L. Hershberger, and F. Gabbard, *Phys. Rev. C* **35**, 1265 (1987).
- [21] T. Sauter and F. Kaeppler, *Phys. Rev. C* **55**, 3127 (1997).
- [22] J. Bork, H. Schatz, F. Käppeler, and T. Rauscher, *Phys. Rev. C* **58**, 524 (1998).
- [23] F. R. Chloupek, A. StJ. Murphy, R. N. Boyd, A. L. Cole, J. Görres, R. T. Guray, G. Raimann, J. J. Zach, T. Rauscher, J. V. Schwarzenberg, P. Tischhauser, and M. C. Wiescher, *Nucl. Phys.* **A652**, 391 (1999).
- [24] S. Harissopoulos, S. Galanopoulos, P. Tsagari, P. Demetriou, G. Kuburas, T. Paradellis, R. Kunz, J. W. Hammer, G. Gyürky, E. Somorjai, S. Goriely, S. Kasemann, A. Dewald, and K. O. Zell, *Nucl. Phys.* **A688**, 421 (2001).
- [25] E. Somorjai, Zs. Fülöp, A. Z. Kiss, C. E. Rolfs, H.-P. Trautvetter, U. Greife, M. Junker, S. Goriely, M. Arnould, M. Rayet, T. Rauscher, and H. Oberhummer, *Astron. Astrophys.* **333**, 1112 (1998).
- [26] Zs. Fülöp, Á. Z. Kiss, E. Somorjai, C. E. Rolfs, H. P. Trautvetter, T. Rauscher, and H. Oberhummer, *Z. Phys. A* **355**, 203 (1996).
- [27] S. Harissopoulos, E. Skreti, P. Tsagari, G. Souliotis, P. Demetriou, T. Paradellis, J. W. Hammer, R. Kunz, C. Angulo, S. Goriely, and T. Rauscher, *Phys. Rev. C* **64**, 055804 (2001).
- [28] Gy. Gyürky, E. Somorjai, Zs. Fülöp, S. Harissopoulos, P. Demetriou, and T. Rauscher, *Phys. Rev. C* **64**, 065803 (2001).
- [29] J. F. Ziegler and J. P. Biersack, Code SRIM, Version 2000.39. Full description given by J. F. Ziegler, J. P. Biersack, and U. Littmark, *The Stopping and Range of Ions in Solids* (Pergamon, New York, 1985).
- [30] G. Amsel and D. David, *Rev. Phys. Appl.* **4**, 383 (1969).
- [31] *Handbook of Chemistry and Physics, CRC*, 64th ed., edited by R. C. Weast (CRC, Boca Raton, FL, 1983).
- [32] R. Kunz, M. Jaeger, A. Mayer, J. W. Hammer, G. Staudt, S. Harissopoulos, and T. Paradellis, *Phys. Rev. Lett.* **86**, 3244 (2001).
- [33] A. Anttila, J. Keinonen, M. Hautala, and I. Forsblom, *Nucl. Instrum. Methods* **147**, 501 (1977).
- [34] P. M. Endt, C. Alderliesten, F. Zijderhand, A. A. Wolters, and A. G. M. Van Hees, *Nucl. Phys.* **A510**, 209 (1990).
- [35] K. Debertin and R. G. Helmer, *Gamma- and X-Ray Spectrometry with Semiconductor Detectors* (North-Holland, Amsterdam, 1988).
- [36] R. B. Firestone, V. S. Shirley, C. M. Baglin, J. Zipkin, and S. Y. F. Chu, *Table of Isotopes*, 8th ed. (Wiley-Interscience, New York, 1996).
- [37] D. C. Camp and A. L. Van Lehn, *Nucl. Instrum. Methods* **76**, 192 (1969).
- [38] S. Goriely, in *Nuclei in the Cosmos V*, edited by N. Prantzos and S. Harissopoulos (Edition Frontières, Paris, 1998), p. 314 (also see <http://www-astro.ulb.ac.be>).
- [39] G. Audi and A. H. Wapstra, *Nucl. Phys.* **A595**, 409 (1995).
- [40] S. Goriely, F. Tondeur, and J. M. Pearson, *At. Data Nucl. Data Tables* **77**, 311 (2001).
- [41] P. Demetriou and S. Goriely, *Nucl. Phys.* **A688**, 584 (2001).
- [42] P. Demetriou and S. Goriely, *Nucl. Phys.* **A695**, 95 (2001).
- [43] C. Grama and S. Goriely, in *Nuclei in the Cosmos V*, edited by N. Prantzos and S. Harissopoulos (Edition Frontières, Paris, 1998), p. 463.
- [44] S. Goriely, *Phys. Lett. B* **436**, 10 (1998).
- [45] J. Kopecky and R. E. Chrien, *Nucl. Phys.* **A468**, 285 (1987).
- [46] Reference Input Parameter Library, IAEA-Tecdoc-1034 (1998) (also see <http://iaeand.iaea.or.at/ripl>).
- [47] J. P. Jeukenne, A. Lejeune, and C. Mahaux, *Phys. Rev. C* **16**, 80 (1977).
- [48] E. Bauge, J. P. Delaroche, and M. Girod, *Phys. Rev. C* **63**, 024607 (2001).
- [49] A. Koning and J. P. Delaroche, *Nucl. Phys. A* (to be published).
- [50] F. D. Becchetti and G. W. Greenlees, *Phys. Rev.* **182**, 1190 (1969).
- [51] S. Goriely, in *Proceedings of the International Conference on Nuclear Data for Science and Technology ND2001, October 2001, Tsukuba, Ibaraki, Japan*, edited by K. Shibata [*J. Nucl. Sci. Technol.* **2**, 536 (2002)].
- [52] F.-K. Thielemann, M. Arnould, and J. W. Truran, in *Advances in Nuclear Astrophysics*, edited by E. Vangioni-Flam, J. Audouze, M. Cassé, J.-P. Chieze, and J. Tran Thanh Van (Editions Frontières, Gif-sur-Yvette, 1986), p. 525.
- [53] S. Goriely, *Nucl. Phys.* **A605**, 28 (1996).
- [54] T. Rauscher and F.-K. Thielemann, *At. Data Nucl. Data Tables* **79**, 47 (2001) (also see <http://quasar.physik.unibas.ch/tommy/reaclib.html>).
- [55] P. Möller, J. R. Nix, W. D. Myers, and W. J. Swiatecki, *At. Data Nucl. Data Tables* **59**, 185 (1995).
- [56] T. Rauscher, F.-K. Thielemann, and K.-L. Kratz, *Phys. Rev. C* **56**, 1613 (1997).